Indonesian Journal of Electrical Engineering and Computer Science
Vol. 34, No. 3, June 2024, pp. 1787~1799
ISSN: 2502-4752, DOI: 10.11591/ijeecs.v34.i3.pp1787-1799

Improved vigenere using affine functions surrounded by two genetic crossovers for image encryption

Hamid El Bourakkadi[1], Abdelhakim Chemlal[1], Hassan Tabti[2], Mourad Kattass[1], Abdellatif Jarjar[1], Abdelhamid Benazzi[1]
[1]MATSI Laboratory, Mohammed First University, Oujda, Morocco
[2]LSIA Laboratory, Sidi Mohamed Ben Abdellah University, Fez, Morocco

Article Info

Article history:

Received Jan 31, 2024
Revised Feb 19, 2024
Accepted Feb 23, 2024

Keywords:

Chaotic map
Genetic crossover
Hybrid circuit
Pseudorandom functions
S-Box

ABSTRACT

This paper presents an improved method for encrypting color images, surpassing the effectiveness of genetic crossover and substitution operations. The technique incorporates dynamic random functions to enhance the integrity of the resulting vector, increasing temporal complexity to thwart potential attacks. The improvement involves integrating genetic crossover and utilizing two extensive pseudorandom replacement tables derived from established chaotic maps in cryptography. Following the controlled vectorization of the original image, our approach initiates with a first genetic crossover inspired by deoxyribonucleic acid (DNA) behavior at the pixel level. This genetic crossover is succeeded by a confusion-diffusion lap, reinforcing the connection between encrypted pixels and their neighboring counterparts. The confusion-diffusion process employs dynamic pseudorandom affine functions at the pixel level. Then a second genetic crossover operator is applied. Simulations conducted on a diverse set of images with varying sizes and formats showcase the robustness of our method against statistical, brute-force, and differential attacks.

Corresponding Author:

Hamid El Bourakkadi
MATSI Laboratory, Mohammed First University
Oujda, Morocco
Email: hamid.elbourakkadi.d23@ump.ac.ma

1. INTRODUCTION

Ensuring the security of information during network transmission has become a widely explored research area. In this context, encryption technology plays a crucial role, with symmetric and asymmetric encryption algorithms applied in cryptography [1]. Symmetric encryption, known for its efficiency, heightened security, and rapid encryption speed with a large key, relies on preserving the ciphering key for its security. The algorithm involves minimal computation and ensures a high protection level and ciphering speed when utilizing a lengthy key. Data security transmission is contingent upon safeguarding the encryption key. On the other hand, while offering high security, asymmetric ciphering comes with significant encryption and decryption time, making it suitable for limited data encryption such as passwords. The security of data transmission in this case relies on both the key and the algorithm. With the principle of Kirchhoff, the key system's protection is closely related to the ciphering key rather than the algorithm. In addressing these challenges, numerous image ciphering methods utilize the principles of symmetry theory, and this paper similarly embraces a strategy centered on the same type of algorithms.

Despite researchers' efforts to develop more secure ciphering methods, numerous image encryption methods have been successfully compromised [2], [3]. In pursuit of heightened security, many scholars have turned to multi-round encryption methods [4], [5], though this approach involves a significant amount of time. Some authors have suggested encryption methods focused solely on the relevant characteristics in an image [6]-[8]. Hussain *et al.* [7] introduced a ciphering architecture for medical images centered on TetraVex game theory method, demonstrating flexibility and reliability in protecting medical images against any attack. Çelik and Doğan [9], suggested an encryption image architecture using data hiding and logistic maps, exhibiting satisfactory security performance in experimental results. Drawing inspiration from these studies, we propose utilizing existing technology to recognize the facial contour area when encrypting human images, enabling the individual encryption of these regions. After encrypting the facial part, the entire image undergoes another layer of encryption. Compared to traditional one-round encryption, this approach demonstrates superior encryption effectiveness. Even in the event of an algorithmic attack, the private aspects, such as the face, remain indistinguishable and unrecoverable. In contrast to multi-round encryption schemes, these techniques involve shorter periods and higher speeds to encrypt and decrypt data.

As chaos theory continues to evolve, researchers have systematically explored the attributes of pseudorandomness, and sensitivity to initial values [10], [11]. Additionally, various chaotic image encryption algorithms have emerged, integrating principles from diverse disciplines such as genetic algorithms rules such as quantum maps and perceptron-like networks [12], [13]. Chatterjee *et al.* [14], Chatterjee et al designed an encryption architecture that involves replacement-diffusion operation using standard and logistic maps, addressing the issue of dynamic degradation. Li *et al.* [15] demonstrate that the use of chaotic sequences as keys can compromise the algorithm's security. Efficiently, chaotic methods have various variations, with some, such as the PWLCM, logistic, Henon, and skew tent maps [16]-[19], being renowned for image encryption. Focusing on the logistic and PWLCM maps, they offer several advantages, including enhanced sensitivity and randomness, resulting in more secure, chaotic, and unique sequences.

The difficulty arises from the dependence of such algorithms on independent block encryption without the intervention of plaintext blocks, making them vulnerable to statistical and frequency attacks. Additionally, without the incorporation of diffusion and chaining functions between the encrypted and plaintext blocks, these classical techniques remain susceptible to differential attacks.

Our contribution to addressing anomalies raised in conventional research has driven us to develop a new image encryption system using two large substitution matrices generated from two chaotic maps highly sensitive to initial conditions, incorporating pseudo-random affine functions for confusion and diffusion restoration. This process is surrounded by two deep genetic crossover operations specifically tailored for image encryption to increase the complexity of attacks against our innovative system. Simulations results and comparisons with other algorithms conducted on randomly selected images from SIPI database reveal a high level of robustness, making our new technique impervious to differential and statistical attacks.

This research paper is divided into various sections, including a section describing the proposed method, explaining the basis of chaotic sequences, the classical Vigenere and affine techniques as well as detailing keys generation axis, revealing the nuances of the encryption and decryption process; a section devoted to results and discussions, presenting research results and discussion; and a section summarizing the findings and proposing research directions.

2. PROPOSED METHOD

Our approach enhances the traditional Vigenere method by incorporating extensive substitution tables alongside novel pseudorandom functions. Furthermore, reversible functions have been seamlessly integrated into the encryption process. However, this technique is divided into four main axes, the used chaotic sequences and functions, different keys generation steps, and the encryption and decryption axes.

2.1. Axis 1: used chaotic sequences and functions

The selected chaotic maps to construct different subkeys for encryption and decryption processes are highly sensitive to initial conditions and easy to implement in a cryptographic system. Additionally, our system incorporates random functions into classical Vigenere method. However, this subsection is divided into four subtitles.

2.1.1. PWLCM map

The first chaotic sequence will be generated by the PLWCM map [16] as defined by (1).

$$h_{n+1} = f(h_n) = \begin{cases} h_0 \in \,]0\,;1[\,, k \in \,]0{,}5;4[\\ k^{-1}\, h_n \; if \; 0 < h_n < k \\ (0{,}5-k)^{-1}(h_n - k)\ \mathrm{k} < h_n < 0{,}5 \\ f(1-h_n)\ \text{otherwise} \end{cases} \quad (1)$$

The parameters (h_0) and (k) represent the initial state and its control parameter, respectively.

2.1.2. Logistic map

The logistic map [17] is a widely used mathematical function that models population growth over time within a limited space. It is a common tool in chaos theory and cryptography. The expression of such map is depicted in (2).

$$\begin{cases} l_0 \in]0{,}5;1[\ et\ \delta \in [3{,}75;4] \\ \quad l_{n+1} = \delta . l_n(1-l_n) \end{cases} \tag{2}$$

2.1.3. Classical Vigenere method

The classical Vigenere cipher system is based on a matrix (M) of fixed dimensions $(26{,}26)$ reserved for text encryption only. The encryption and decryption algorithms associated with the classical Vigenere method are given in Algorithm 1.

Algorithm 1. Classical Vigenere encryption and decryption algorithms

```
//Encryption
$for\ i = 1\ to\ n$
    $Ck_i = M(Ck_i, Ke_i) = Pk_i + Ke_i\ mod\ 26$
$end\ for$

//Decryption
$for\ i = 1\ to\ n$
    $Pk_i = M^{-1}(Pk_i, Ke_i) = Ck_i - Ke_i\ mod\ 26$
$end\ for$
```

Where (Pk) is the plain message, (Ck) is the cipher message, (Ke) is the encryption key, (M) is the vigenere matrix, and (n) be the length of the plain message.

2.1.4. Affine functions in (Z/nZ)

Let (f) be an affine function defined in the ring (Z/nZ) by (3).

$$\begin{cases} \quad f: Z/nZ \ \rightarrow \ Z/nZ \\ x \ \longmapsto \ mod(ax+b;n) \end{cases} a, b \in \ Z/nZ \tag{3}$$

The function (f) is a bijective function in (Z/nZ) if and only if (a) is invertible and (b) is any.
Indeed, we have $y = mod(ax+b;n)$
Then, $ax = mod(y-b;n)$ and $x = mod(a^{-1}.(y-b);n)$ Where (a^{-1}) is the inverse of (a) in ring (Z/nZ).
Or, we know that (a) is invertible in (Z/nZ) if and only if $a \wedge n = 1$.
Particular case: $n = 2^k, k \in N$
In a particular case**,** (a) is invertible in ring $(Z/2^kZ)$ if and only if (a) is odd.

2.2. Axis 2: keys generation

This new technique uses the two most widely deployed chaotic maps in the field of cryptography [18], [19] by integrating large S-boxes incorporating strong pseudorandom affine functions for the confusion-diffusion process. The confusion-diffusion process is encapsulated by two genetic crossovers. This technique is structured around the subsections described below.

2.2.1. Pseudorandom vectors generation

Our system is a cryptographic architecture that necessitates the generation of subkeys. These subkeys are generated from two chaotic sequences that are extremely sensitive to initial conditions. The below subsections detail such process.

2.2.2. Used chaotic sequences

Two chaotic sequences (h) and (l) were generated based on PWLCM and Skew tent chaotic maps described in sub section (3.1). These sequences, used in our approach, are extremely sensitive to the initial conditions and easy to implement in any cryptosystem.

2.2.3. Sub keys construction

Seven pseudorandom vectors $(Vc1)$, $(Vc2)$, $(Vc3)$, (Vr), (Ve), (Va), and (Vb) with coefficients in the ring $(Z/256Z)$ are generated by Algorithm 2.

Algorithm 2. Pseudorandom vectors generation

```
$for\ i\ =\ 1\ to\ 3nm$
    Vc1( i)= [E(max(h(i);l(i)).$10^{11}$ ) mod 253]+2 // First confusion vector
    $Vc2(\ i) =\ [E(((h(i) + 2 * l(i))/3).10^{11})\ mod\ 254] + 1$ // Second confusion vector
```

$Vc3(\,i) = \ [E(|h(i) - l(i)|.\,10^{10}\,)\ mod\ 254] + 1$ // Third confusion vector
$Vr(\,i) = \ \left[E\big((h(i) + l(i)).\,10^{12}\big)\ mod\ 253\right] + 2$ // First translation vector
$Ve(\,i) = \ \left[E\left(\left(\frac{2*h(i)+3*l(i)}{5}\right).\,10^{12}\right)\ mod\ 253\right] + 2$ // Second translation vector
$Va(i) = \left[2 * E\big((h(i) + l(i)).\,10^{12}\big) + 1\right] mod\ 256$ // First multiplication vector
$Vb(i) = \left[2 * E\big((h(i) * l(i)).\,10^{12}\big) + 1\right] mod\ 256$ // Second multiplication vector : $end\ for$

The two vectors (Va) and (Vb) contain only the invertible elements in the ring ($Z/256Z$). In addition, our system requires the generation of three binary vectors, ($Ba1$), ($Ba2$), and ($Ba3$), to control the encryption process. These two vectors are generated by Algorithm 3.

Algorithm 3. (Ba_i) Binary random vectors generation, $i\in\{1, 2, 3\}$

```
//Binary vectors construction
$for\ i \leftarrow 1\ to\ 3nm$
 $if\ h(i) > l(i)\ then$
 $Ba1(i)\ \leftarrow 0$
 $else : Ba1(i)\ \leftarrow 1$
 $end\ if$
 $if\ h(i) > 0,5\ then : Ba2(i)\ \leftarrow 0$
$else :\ Ba2(i)\ \leftarrow 1$
$end\ if$
$if\ h(\,i\,)\ \leq l(i)\ then$
$Ba3(i)\ \leftarrow\ 0$
$else :\ Ba3(i)\ \leftarrow 1$
$end\ if$
$end\ for$
```

2.2.4. Generation of genetic crossover table (GC)

This operation is a genetic crossover adapted to the encryption of color images that will be accompanied by a table (GC) of size (3nm,2). The construction of this table is given by the steps below:
- The 1st column is the arrangement (P) obtained by a decreasing sort on the first (3nm) values of the sequence (h).
- The second column is the permutation (P') obtained by an increasing sort on the first (3nm) values of the sequence (l).

2.2.5. Substitution tables generation

Our algorithm necessitates the creation of two novel tables, denoted as ($M1$) and ($M2$). These tables are used in confusion/difusion process as substitution matrices. Each table is sized at (256; 256) and operates with coefficients within the ring (Z/nZ).

2.2.6. ($M1$) S-BOX generation

The main mission of this section is to construct the new Vigenere substitution matrix, called ($M1$), with a size of ($256; 256$), following the instructions provided below.
- The first row of the table ($M1$) is the permutation ($Pt1$) of the first 256 values of the vector ($Vc1$), obtained by sorting them in decreasing order.
- For ranks higher than 1, the rank line is a rank shift $Vc2(i)$ or $Vc3(i)$, depending on the control vector $Ba1(i)$. This table was generated by Algorithm 4.

Algorithm 4. (M1) Substitution box generation

```
$for\ i \leftarrow\ 1\ to\ 256\ //\ First\ line$
 $M1(1, i)\ \leftarrow\ Pt1(i)$
$end\ for$
$for\ i \leftarrow\ 2\ to\ 256\ //\ Next\ lines$
        $for\ j \leftarrow\ 1\ to\ 256$
$if\ Ba1(i) = 0\ then$
$M1(i, j)\ \leftarrow\ M1(i-1, mod(j + Vc2(i), 256))$
$else$
$M1(i, j)\ \leftarrow\ M1(i-1, mod(j + Vc3(i), 256))$
$end\ if : end\ for : end\ for$
```

2.2.7. ($M2$) S-BOX generation

The construction of the new substitution matrix ($M2$) of size (256;256) is described by:
- The 1st line is the rearrangement ($Pr1$) obtained by a broad ascending order on the first 256 values of the vector ($Vc3$);
- The 2nd line is the rearrangement ($Pr2$) obtained by a broad ascending order on the first 256 values of the vector ($Vc2$);
- The 3rd line is the rearrangement ($Pr3$) obtained by a broad ascending order on the first 256 values of the vector ($Vc1$);
- The ith line ($i > 3$) is the composition of the functions of row ($i - 2$) and ($i - 3$) or ($i - 3$) and ($i - 1$), depending on the value of the control vector $Ba2(i)$.

These steps are illustrated in Algorithm 5.

Algorithm 5. (M2) Substitution box generation

```
$for\ i\ \leftarrow\ 1\ to\ 256$ //3 first lines
$for\ i\ \leftarrow\ 4\ to\ 256$ //Next lines
```

```
$M2(1,i) \leftarrow Pr1(i)$
$M2(2,i) \leftarrow Pr2(i)$
$M2(3,i) \leftarrow Pr3(i)$
$end\ for$
$for\ j \leftarrow 1\ to\ 256$
    $if\ Ba2(i) = 0\ then : M2(i,j) \leftarrow M2(i-2, M2(i-3,j))$
    $else: M2(i,j) \leftarrow M2(i-3, M2(i-1,j))$
    $end\ if: end\ for : end\ for$
```

2.3. Axis 3: encryption phase

The innovative encryption process improves upon the traditional Vigenere technique by incorporating enhanced methods. It utilizes dynamic functions for confusion and diffusion, adding a unique twist to the Vigenere method. Additionally, two genetic mutations specifically designed for encrypting color images complement this approach. The process is organized into the following stages:

2.3.1. Original image vectorization

This phase involves uploading the original image of dimensions (n, m) and then extracting the (RGB) channel vectors (R), (G), and (B), which are concatenated under the control of the binary vector (Ba1) into a single vector (XD) of dimensions $(1,3nm)$. The mathematical formulation of this phase is described in Algorithm 6.

Algorithm 6. Original image vectorization algorithm

```
$for\ j \leftarrow 1\ to\ nm$
    $if\ Ba1(j) = 0\ then$
        $XD(3j-2) \leftarrow R(j) \oplus Vc1(j)$
        $XD(3j-1) \leftarrow G(j) \oplus Vc2(j)$
        $XD(3j) \leftarrow B(j) \oplus Vc3(j)$
    $else$
        $XD(3j-2) \leftarrow R(j) \oplus Vc3(j)$
        $XD(3j-1) \leftarrow G(j) \oplus Vc1(j)$
        $XD(3j) \leftarrow B(j) \oplus Vc2(j)$
    $end\ if : end\ for$
```

2.3.2. First genetic crossover operation

After image preparation above, the genetic crossover will be applied to the integrity of the output vector (XD). This operation will be subject to the control of the table $(GC1)$ and given by (4).

$$X(i) = XD(GC1(i,1)) \oplus Vc1(GC1(i,2)), i \in [1, 3nm] \tag{4}$$

The first column of the table $(GC1)$ indicates the rank of the pixel to be modified, while its second column indicates the rank of the chaotic value chosen for the confusion. This algorithm is illustrated by the following Figure 1. The first column of the table $(GC1)$ indicates the rank of the pixel to be modified, while its second column indicates the rank of the chaotic value chosen for the confusion.

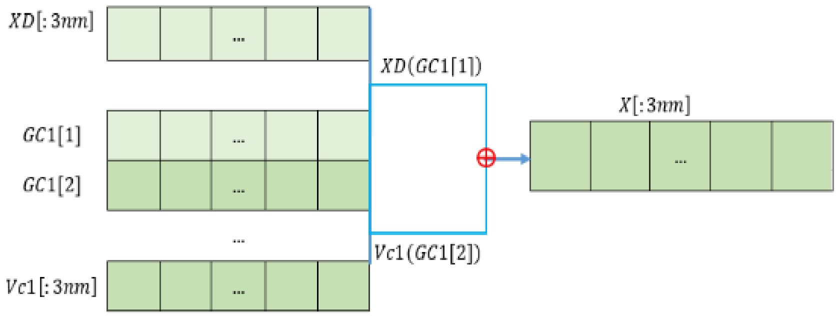

Figure 1. First genetic crossover operation

2.3.3. Confusion and diffusion process

a. Expression of the pseudorandom functions

Let (f_i) be the family of affine functions acting on the pixels. These functions are defined by (5).

$$\begin{cases} f_i: Z/256Z \rightarrow Z/256Z \\ x \mapsto \begin{cases} mod(Va(i) * X(i) + Ve(i); 256)\ si\ Ba2(i) = 0 \\ mod(Vb(i) * X(i) + Vr(i); 256)\ si\ Ba2(i) = 1 \end{cases} \end{cases} \tag{5}$$

Since the elements $Va(i)$ and $Vb(i)$ are invertible in ring **$(Z/256Z)$,** the functions (f_i) are reversible for all $i \in [1;\ 3nm]$.

b. Confusion and diffusion function expression

To enhance the security of our system against potential differential attacks, we're incorporating confusion and diffusion functions that utilize pseudo-random vectors and reversible dynamic functions. This chaining technique involving replacement tables ($M1$) and ($M2$) amplifies the avalanche effect. The execution of diffusion functions is outlined in Algorithm 7.

Algorithm 7. (Fv) confusion and diffusion function expression

```
$Z(i) = Fv(X(i))$
$if\ Ba2(i) = 0\ then: Z(i) \leftarrow M1(Vc1(i), M2(Vc2(i); mod(Va(i) * X(i) + Ve(i); 256)))$
$else : Z(i) \leftarrow M2\big(Vc3(i), M1(Vc1(i);\ mod(Vb(i) * X(i) + Vr(i); 256))\big)$
$end\ if$
```

c. Initialization value calculation

This improved Vigenere lap starts by calculating the initialization value (In), which is closely linked to the plain image and is intended to change the value of the starting pixel and launch the encryption phase. This value is calculated by Algorithm 8 below.

Algorithm 8. Initialization value calculation

```
$In = 0$
$for\ i = 2\ to\ 3nm$
    $if\ Ba3(i) = 0\ then$
        $In = In \oplus X(i) \oplus Vc2(i)$
    $else$
        $In = In \oplus X(i) \oplus Vc3(i)$
    $end\ if$
$end\ for$
```

This algorithm is illustrated in Figure 2 below.

d. Confusion and diffusion circuit

To overcome any differential attack, we first perform a diffusion round using the chaotic confusion vectors and a chaining between the ciphered pixels and the following plain pixels using the bijective affine functions. The diffusion process is illustrated by Algorithm 9.

Algorithm 9. Confusion and diffusion circuit

```
//First pixel encryption
$Z(1) = Fv(X(1) \oplus In \oplus Vc1(1))$
//Next pixels encryption
$for\ i = 2\ to\ 3nm$
    $\alpha = f_i(X(i)) \oplus Z(i-1)$
    $if\ Ba3(i) = 0\ then : Z(i) = Fv(\alpha \oplus Vc2(i))$
    $else : Z(i) = Fv(\alpha \oplus Vc3(i))$
    $end\ if$
$end\ for$
```

This algorithm can be interpreted in Figure 2.

2.3.4. Second genetic crossover operation

After image preparation above, the genetic crossover will be applied to the integrity of the output vector (Z). This operation will be subject to the control of the table ($GC2$) and given by (6).

$$T(\,i) = Z(GC2(i,1)) \oplus Vc2(GC2(i,2))\,, i \in [1\,, 3nm] \tag{6}$$

The first column of the table ($GC2$) indicates the rank of the pixel to be modified, while its second column indicates the rank of the chaotic value chosen for the confusion. This algorithm is illustrated by the following Figure 3.

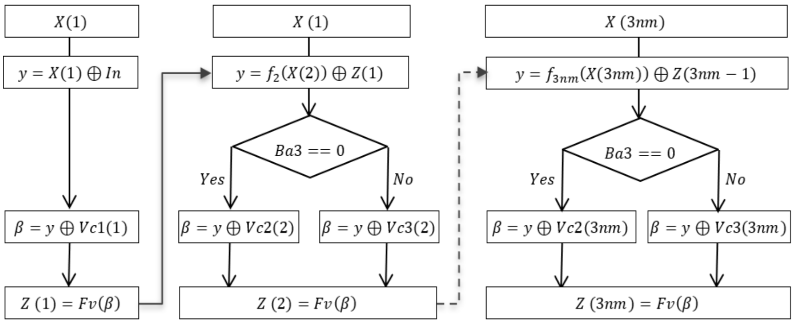
$X(1)$
$y = X(1) \oplus In$
$\beta = y \oplus Vc1(1)$
$Z\ (1) = Fv(\beta)$
$X\ (1)$
$y = f_2(X(2)) \oplus Z(1)$
$Ba3 == 0$
Yes
No
$\beta = y \oplus Vc2(2)$
$\beta = y \oplus Vc3(2)$
$Z\ (2) = Fv(\beta)$
$X\ (3nm)$
$y = f_{3nm}(X(3nm)) \oplus Z(3nm-1)$
$Ba3 == 0$
Yes
No
$\beta = y \oplus Vc2(3nm)$
$\beta = y \oplus Vc3(3nm)$
$Z\ (3nm) = Fv(\beta)$

Figure 2. New Hybrid circuit incorporating dynamic pseudorandom affine functions

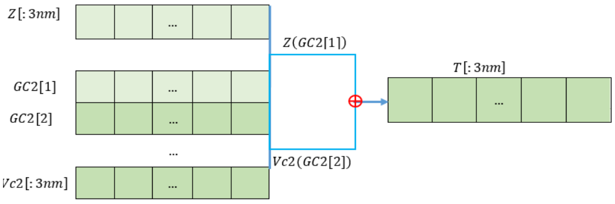

Figure 3. Second genetic crossover operation

The first column of the table ($GC2$) indicates the rank of the pixel to be modified, while its second column indicates the rank of the chaotic value chosen for the confusion. The resulting vector (T) represents the cipher image.

2.4. Axis 4: phase of decryption

The suggested encryption system is symmetric and employs two diffusion functions, necessitating that the decryption process commences by applying the inverse functions to the last operation. The encrypted image transforms a vector (Z) with dimensions (1; 3nm), upon which the subsequent steps are carried out:

- Application of the reverse for the second genetic crossover operation.
- Inverse of the pseudorandom functions and inverse of the confusion and diffusion circuit;
- Application of the reverse for the first crossover operation.

3. RESULTS AND DISCUSSION

All the simulations were implemented in Python on the Windows 10 operating system with a hardware environment consisting of an i7 processor laptop, a 1 TB hard drive, and 32 GB of RAM. The main test image "Lena", as well as its encrypted and decrypted images, as well as all the plain images we used, were taken from SIPI database [20]. These image samples. The keys and other experimental parameters are generated from the chaotic maps described above. Prior to initiating the decryption process, the secret key needs to be securely transmitted to the recipient through a protected channel.

3.1. Statistical attacks

Examining encrypted data to reveal details about the encryption key or the plaintext images constitutes a statistical attack. These assaults encompass histogram attacks, entropy attacks, and correlation attacks, among others. The subsequent subsections delineate the impacts of these assaults on our system.

3.1.1. Analysis of possible keys space

Our algorithm uses two chaotic maps generated by four real parameters represented by 32 bits each. So, the size of our key is equal to 128 bits and encompasses 120 bits. This ensures that our system is resistant to any brute-force attack.

3.1.2. Key strength analysis

Our system uses two of the most widely utilized chaotic maps in the field of cryptography. Because they are highly sensitive to initial conditions, this guarantees significant responsiveness to our encryption key. This can be seen in the diagram in Figure 4. So, any modification of the encryption key will lead to two different ciphered images being obtained during the encryption stage. In addition, two decrypted images across the decryption stage will have completely different shapes. This confirms that our cryptosystem is safe from any brute-force attack.

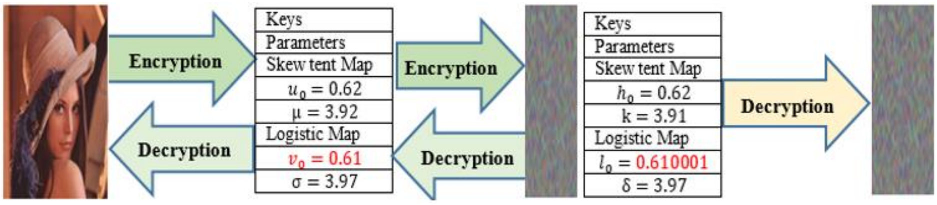

Figure 4. Key strength analysis

3.1.3. Analysis of histograms

Histograms of images showing the distribution of pixel values. Figures 5 (a) to (d) illustrate the RGB histograms of all the test images used, while Figures 6 (a) to (d) show the RGB histograms of the corresponding encrypted images by our method. It is observable that the histograms of encrypted images generated by our system are almost uniformally distributed. This ensures better protection against any statistical attack.

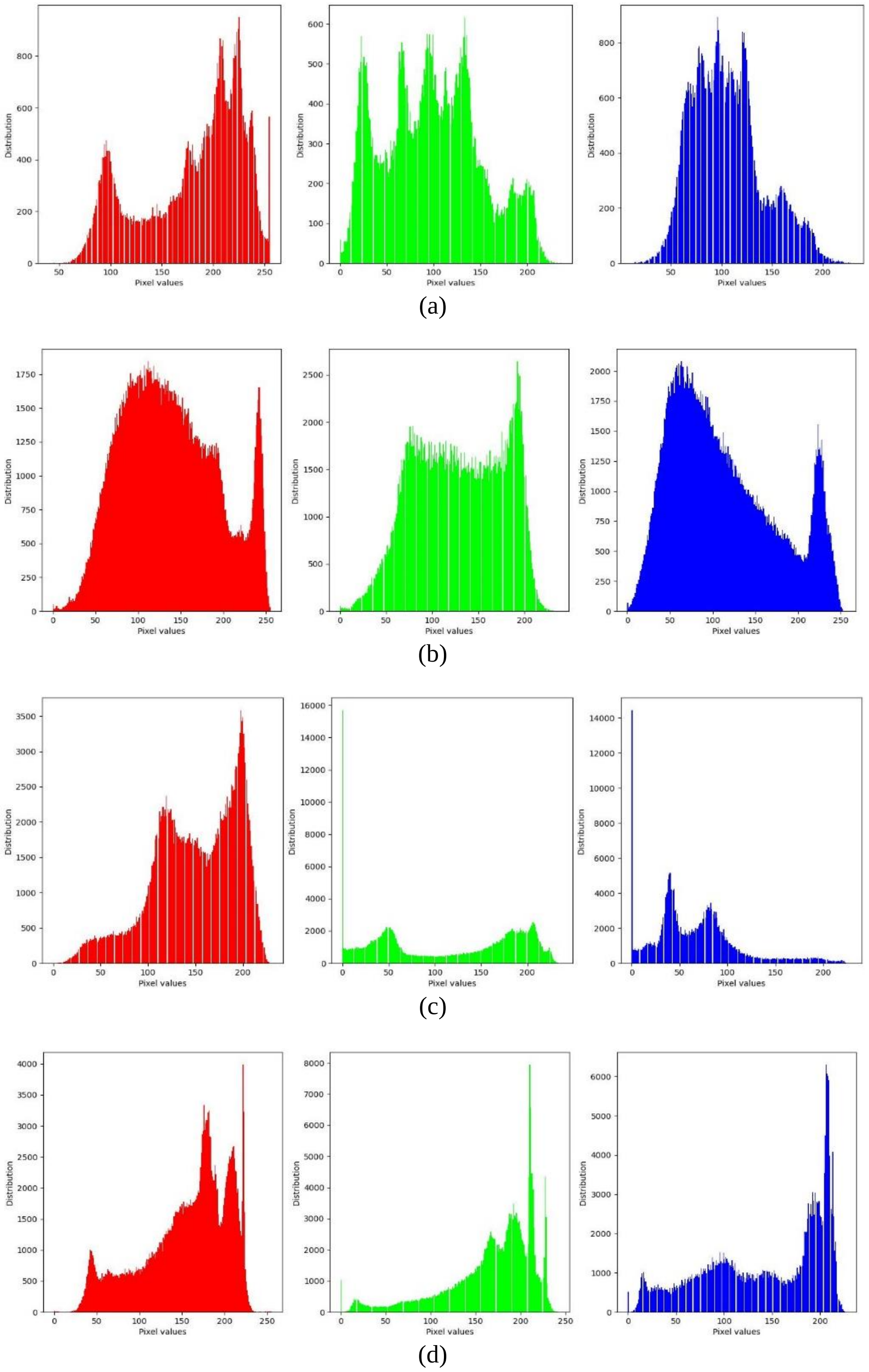

(a)

(b)

(c)

(d)

Figure 5. RGB histograms of the original images (a) histogram of Lena plain image, (b) histogram of baboon plain image, (c) histogram of peper plain image and (d) histogram of house plain image

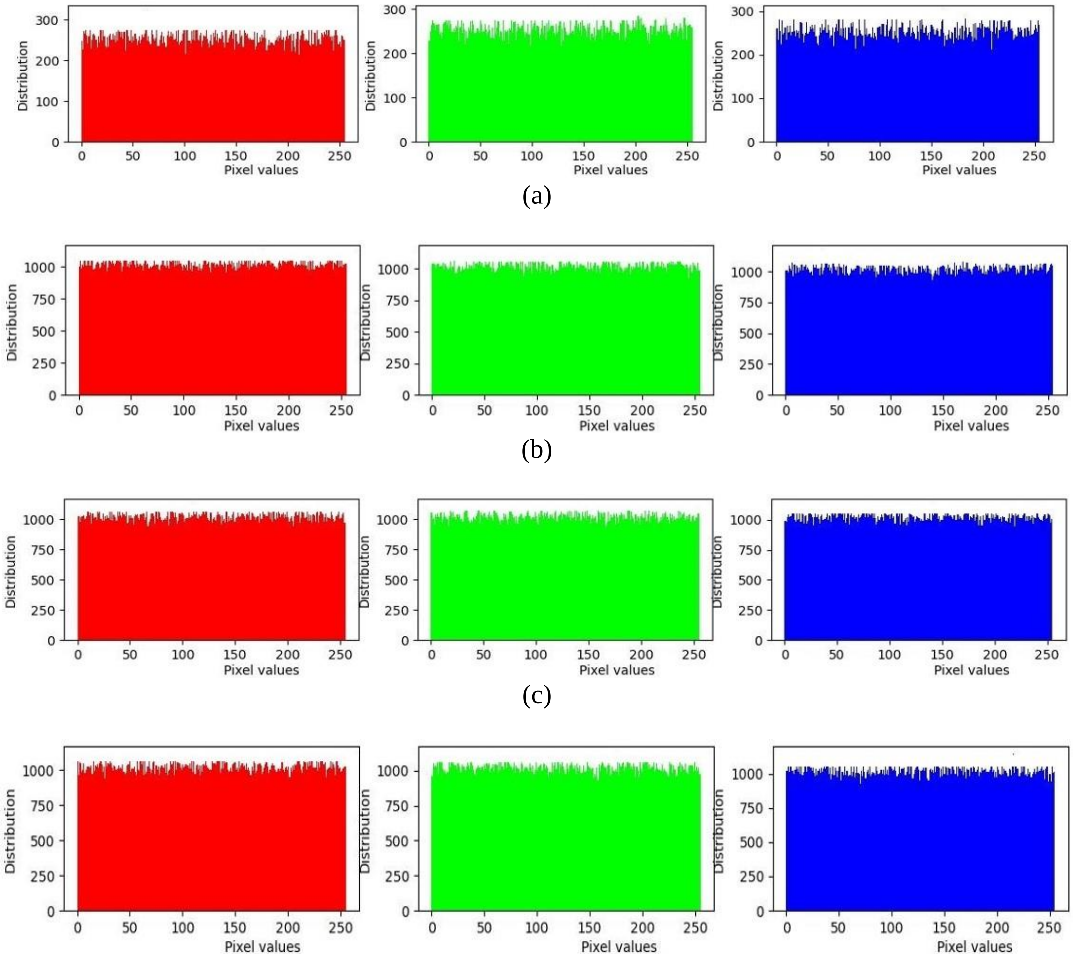

(a)

(b)

(c)

(d)

Figure 6. RGB histograms of the encrypted images by our method (a) histogram of lena encrypted image, (b) histogram of baboon encrypted image, (c) histogram of peper encrypted image and (d) histogram of house encrypted image

3.1.4. Analysis of entropy

The entropy of an image of size (n, m) serves as a metric for assessing the security of that image encryption is given by (7).

$$S(MC) = \frac{-1}{3nm}\sum_{i=1}^{3nm} p(i).log_2(p(i)) \qquad (7)$$

Where $p(i)$ represents the probability of occurrence of level (i) in the plain image.

Table 1 illustrates a comparison between our approach and some similar approaches. This comparison proves that our approach is significantly better than the other compared algorithms [21]-[23]. This confirms that our cryptosystem can withstand entropy image attack.

Table 1. Comparison of encrypted image entropy with other methods: Lena (L), peppers (Pe), House (H)

Algorithm	Images		Encrypted	
		Red	Green	Blue
Proposed	Lena	7,9975	7,9975	7,9974
	Peppers	7,9995	7,9995	7,9996
[21]	Lena	7,9972	7,9973	7,9970
	Peppers	7,9993	7,9994	7,9994
[22]	Lena	7,9730	7,9750	7,9710
[23]	Lena	7.9974	7,9974	7,9971
	Peppers	7,9993	7,9994	7,9992

3.1.5. Correlation analysis

In (8) provides the correlation of an image with dimensions (n, m).

$$corr = \frac{cov(x,y)}{\sqrt{var(x)}.\sqrt{var(y)}} \tag{8}$$

Table 2 illustrates a comparison between our approach and some similar approaches. This comparison proves that our approach is significantly better than the other compared algorithms. This verifies the security of our cryptosystem against statistical attacks. Table 3 illustrates a comparison between our approach and some similar approaches [21], [23], [24]. These results validate the resistance of our cryptosystem to statistical attacks.

Table 2. Correlations between pixels for Lena, Apricot and Panda images

Images		Original image			Encrypted image		
		Horizontal	Vertical	Diagonal	Horizontal	Vertical	Diagonal
Lena	Red	0,95580	0,96480	0,93220	-0,00376	0,00815	-0,00131
	Green	0,93556	0,95756	0,91902	-0,00298	0,00912	-0,00673
	Blue	0,90773	0,93930	0,89130	-0,00145	-0,00672	0,00064
Apricot	Red	0,98385	0,96944	0,98629	-0,00137	-0,00188	-0,00541
	Green	0,97883	0,98511	0,96537	-0,00107	0,00150	0,00234
	Blue	0,99153	0,98348	0,98724	0,00489	-0,00571	-0,00118
Panda	Red	0,95175	0,96552	0,93161	0,00513	-0,00077	-0,00495
	Green	0,95215	0,96436	0,93066	0,00788	-0,00080	0,00027
	Blue	0,95542	0,97086	0,94265	0,00007	0,01097	-0,00106

Table 3. Correlation between ciphered “Lena" pixels

Method	Horizontal	Vertical	Diagonal
Proposed	-0,0027336	0,0035	-0,0024696
[21]	-0,0029883	0,0091357	-0,0067375
[23]	-0,0042707	-0,0032498	-0,0020192
[24]	-0,0098	-0,0050	-0,0013

3.4. Differential attacks

Differential attacks capitalize on differences in input processing within a cryptographic system. They target how the system reacts to minor alterations in plaintext or the key to infer critical details, such as the encryption key. To evaluate the algorithm's performance against such attacks, metrics like the rate of pixel changes (NPCR), the unified average change intensity (UACI).

3.4.1. NPCR and UACI metrics analysis

These metrics can be given by (9) and (10).

$$NPCR = \left(\frac{1}{3nm}\sum_{i,j=1}^{nm} Df(i,j)\right).100 \tag{9}$$

$$UACI = \left(\frac{1}{3nm}\sum_{i,j=1}^{3nm} \frac{|Im_1(i,j)-Im_2(i,j)|}{255}\right).100 \tag{10}$$

Where $Df(i,j) = \begin{cases} 1 & if \quad Im_1(i,j) \neq Im_2(i,j) \\ 0 & if \quad Im_1(i,j) = Im_2(i,j) \end{cases}$, $Im_1(i,j)$ is the first image pixel of rank (i,j) and $Im_2(i,j)$ is the first modified image pixel of rank (i,j).

Table 4 illustrates a comparison between our approach and some similar approaches. This comparison proves that our approach is significantly better than the other compared algorithms [21], [24]-[30]. This validates the resistance of our cryptosystem to differential attacks.

Table 4. Comparison of the NPCR and UACI

Method		Ours	[21]	[24]	[25]	[26]	[27]	[28]	[29]	[30]
Lena	UACI (%)	33,56	33,44	33.45	33.0305	30,3921	33,44	33,65	33,46	33.4685
	NPCR (%)	99,73	99,66	99.63	99.6367	99,5926	99,60	99,62	99,60	99.6092
Peppers	UACI (%)	33,53	33,47	33.46	-	32,1233	-	-	-	-
	NPCR (%)	99,69	99,63	99.61	-	99,5768	-	-	-	-

3.4.2. PSNR metric analysis

MSE stands for mean squared error. (n) denotes the number of rows in the original image, and (m) represents the number of columns in the image. The PSNR is evaluated in decibels and is inversely proportional to the mean squared error. It is determined by (11).

$$PSNR = 10 * log_{10}\left(\frac{(2^L-1)^2}{MSE}\right) (dB) \tag{11}$$

- L=8 denotes the bit depth of the particular image, $MSE = \frac{1}{(3nm)^2}\sum_{i,j=1}^{3nm}|Im_1(i,j) - Im_2(i,j)|^2$
- (Im1) and (Im2) represent the original and encrypted images, respectively

Table 5 illustrates a comparison between our approach and some similar approaches. This comparison proves that our approach is significantly better than the other compared algorithms [23], [31]-[33]. This confirms the resilience of our cryptosystem against any differential attacks.

Table 5. The PSNR (dB) between the original image, the encrypted image, and the decrypted image

	Method	Ours	[23]	[31]	[32]	[33]
Lena	Original to Encrypted	∞	∞	-	-	∞
	Original to decrypted	7,0211	8,1102	8,3655	8,2522	7,0257
Baboon	Original to Encrypted	∞	∞	-	-	∞
	Original to decrypted	7,1721	8,7776	8,8532	8,8223	7,1515

4. CONCLUTION

The obtained statistical and differential constants were evaluated according to international standards. To achieve this, we employed pseudo-random and reversible affine functions in the processes of confusion and diffusion. Additionally, two S-Boxes derived from chaotic maps were incorporated and framed by two specifically adapted genetic crossovers for the encryption of color images. This approach led to the development of a large-scale algorithm ensuring a uniform distribution of histograms for each encrypted image. Consequently, our cryptographic system demonstrates robustness against known attacks, as evidenced by comparisons with several similar algorithms.

REFERENCES

[1] A. M. Alnajim, E. Abou-Bakr, S. S. Alruwisan, S. Khan, and R. A. Elmanfaloty, “Hybrid chaotic-based PRNG for secure cryptography applications,” *Applied Sciences*, vol. 13, no. 13, p. 7768, Jun. 2023, doi: 10.3390/app13137768.

[2] M. Es-Sabry *et al.*, “Securing images using high dimensional chaotic maps and DNA encoding techniques,” *IEEE Access*, vol. 11, pp. 100856–100878, 2023, doi: 10.1109/ACCESS.2023.3315658.

[3] M. U. Rehman, A. Shafique, K. H. Khan, and M. M. Hazzazi, “Efficient and secure image encryption using key substitution process with discrete wavelet transform,” *Journal of King Saud University - Computer and Information Sciences*, vol. 35, no. 7, p. 101613, Jul. 2023, doi: 10.1016/j.jksuci.2023.101613.

[4] C. Maiti, B. C. Dhara, S. Umer, and V. Asari, “An efficient and secure method of plaintext-based image encryption using fibonacci and tribonacci transformations,” *IEEE Access*, vol. 11, pp. 48421–48440, 2023, doi: 10.1109/ACCESS.2023.3276723.

[5] A. Toktas, U. Erkan, S. Gao, and C. Pak, “A robust bit-level image encryption based on Bessel map,” *Applied Mathematics and Computation*, vol. 462, p. 128340, Feb. 2024, doi: 10.1016/j.amc.2023.128340.

[6] J. Zhou, J. Li, and X. Di, “A novel lossless medical image encryption scheme based on game theory with optimized ROI parameters and hidden ROI position,” *IEEE Access*, vol. 8, pp. 122210–122228, 2020, doi: 10.1109/ACCESS.2020.3007550.

[7] M. Hussain, N. Iqbal, and Z. Bashir, “Image pixels swapping encryption based on the TetraVex game and a publicly hash-sharing algorithm,” *Cluster Computing*, Jan. 2024, doi: 10.1007/s10586-023-04226-0.

[8] U. Erkan, A. Toktas, S. Memiş, Q. Lai, and G. Hu, “An image encryption method based on multi-space confusion using hyperchaotic 2D Vincent map derived from optimization benchmark function,” *Nonlinear Dynamics*, vol. 111, no. 21, pp. 20377–20405, Nov. 2023, doi: 10.1007/s11071-023-08859-z.

[9] H. Çelik and N. Doğan, “A hybrid color image encryption method based on extended logistic map,” *Multimedia Tools and Applications*, vol. 83, no. 5, pp. 12627–12650, Jul. 2023, doi: 10.1007/s11042-023-16215-x.

[10] X. Wang and S. Gao, “Image encryption algorithm for synchronously updating Boolean networks based on matrix semi-tensor product theory,” *Information Sciences*, vol. 507, pp. 16–36, Jan. 2020, doi: 10.1016/j.ins.2019.08.041.

[11] P. Huang, D. Li, Y. Wang, H. Zhao, and W. Deng, “A novel color image encryption algorithm using coupled map lattice with polymorphic mapping,” *Electronics*, vol. 11, no. 21, p. 3436, Oct. 2022, doi: 10.3390/electronics11213436.

[12] G. Ye, K. Jiao, and X. Huang, “Quantum logistic image encryption algorithm based on SHA-3 and RSA,” *Nonlinear Dynamics*, vol. 104, no. 3, pp. 2807–2827, May 2021, doi: 10.1007/s11071-021-06422-2.

[13] Y. Zhang, A. Chen, Y. Tang, J. Dang, and G. Wang, “Plaintext-related image encryption algorithm based on perceptron-like network,” *Information Sciences*, vol. 526, pp. 180–202, Jul. 2020, doi: 10.1016/j.ins.2020.03.054.

[14] D. Chatterjee, B. G. Banik, and A. Banik, “Attack resistant chaos-based cryptosystem by modified baker map and logistic map,” *International Journal of Information and Computer Security*, vol. 20, no. 1/2, p. 48, 2023, doi: 10.1504/IJICS.2023.128002.

[15] C. Li, K. Tan, B. Feng, and J. Lu, “The graph structure of the generalized discrete arnold’s cat map,” *IEEE Transactions on Computers*, vol. 71, no. 2, pp. 364–377, Feb. 2022, doi: 10.1109/TC.2021.3051387.

[16] K. K. Raghuvanshi, S. Kumar, S. Kumar, and S. Kumar, “Investigation of piecewise linear chaotic map as a diffusion model for image encryption,” *Multimedia Tools and Applications*, vol. 82, no. 23, pp. 36325–36342, Sep. 2023, doi: 10.1007/s11042-023-15145-y.

[17] H. Khan, M. M. Hazzazi, S. S. Jamal, I. Hussain, and M. Khan, “New color image encryption technique based on three-dimensional logistic map and Grey wolf optimization based generated substitution boxes,” *Multimedia Tools and Applications*, vol. 82, no. 5, pp. 6943–6964, Feb. 2023, doi: 10.1007/s11042-022-13612-6.

[18] Y. Chen, S. Xie, and J. Zhang, “A hybrid domain image encryption algorithm based on improved henon map,” *Entropy*, vol. 24, no. 2, p. 287, Feb. 2022, doi: 10.3390/e24020287.

[19] T. Umar, M. Nadeem, and F. Anwer, “A new modified skew tent map and its application in pseudo-random number generator,” *Computer Standards & Interfaces*, vol. 89, p. 103826, Apr. 2024, doi: 10.1016/j.csi.2023.103826.

[20] A. Weber, “The USC-SIPI image database,” USC Viterbi School of Engineering. Accessed: Feb. 21, 2024. [Online]. Available: https://sipi.usc.edu/database/database.php?volume=misc

[21] S. Khan, H. Lansheng, Y. Qian, H. Lu, and S. Meng Jiao, “Security of multimedia communication with game trick based fast, efficient, and robust color-/gray-scale image encryption algorithm,” *Transactions on Emerging Telecommunications Technologies*, vol. 32, no. 2, Feb. 2021, doi: 10.1002/ett.4034.

[22] X. Wu, K. Wang, X. Wang, H. Kan, and J. Kurths, “Color image DNA encryption using NCA map-based CML and one-time keys,” *Signal Processing*, vol. 148, pp. 272–287, Jul. 2018, doi: 10.1016/j.sigpro.2018.02.028.

[23] K. K. Butt, G. Li, S. Khan, and S. Manzoor, “Fast and efficient image encryption algorithm based on modular addition and SPD,” *Entropy*, vol. 22, no. 1, p. 112, Jan. 2020, doi: 10.3390/e22010112.

[24] S. A. Mahmood, K. A. Hussein, Y. N. Jurn, and E. A. Albahrani, “Parallelizable cipher of color image based on two-dimensional chaotic system,” *Indonesian Journal of Electrical Engineering and Computer Science (IJEECS)*, vol. 18, no. 1, p. 101, Apr. 2020, doi: 10.11591/ijeecs.v18.i1.pp101-111.

[25] H. R. Shakir, S. A. Mehdi, and A. A. Hattab, “A new four-dimensional hyper-chaotic system for image encryption,” *International Journal of Electrical and Computer Engineering (IJECE)*, vol. 13, no. 2, p. 1744, Apr. 2023, doi: 10.11591/ijece.v13i2.pp1744-1756.

[26] W. Alexan, D. El-Damak, and M. Gabr, “Image encryption based on fourier-DNA coding for hyperchaotic chen system, chen-based binary quantization s-box, and variable-base modulo operation,” *IEEE Access*, vol. 12, pp. 21092–21113, 2024, doi: 10.1109/ACCESS.2024.3363018.

[27] A. Yaghouti Niyat, M. H. Moattar, and M. Niazi Torshiz, “Color image encryption based on hybrid hyper-chaotic system and cellular automata,” *Optics and Lasers in Engineering*, vol. 90, pp. 225–237, Mar. 2017, doi: 10.1016/j.optlaseng.2016.10.019.

[28] J. Chen, Z. Zhu, L. Zhang, Y. Zhang, and B. Yang, “Exploiting self-adaptive permutation–diffusion and DNA random encoding for secure and efficient image encryption,” *Signal Processing*, vol. 142, pp. 340–353, Jan. 2018, doi: 10.1016/j.sigpro.2017.07.034.

[29] G. Ye and X. Huang, “An efficient symmetric image encryption algorithm based on an intertwining logistic map,” *Neurocomputing*, vol. 251, pp. 45–53, Aug. 2017, doi: 10.1016/j.neucom.2017.04.016.

[30] C. Chen, D. Zhu, X. Wang, and L. Zeng, “One-dimensional quadratic chaotic system and splicing model for image encryption,” *Electronics*, vol. 12, no. 6, p. 1325, Mar. 2023, doi: 10.3390/electronics12061325.

[31] X. Liu, D. Xiao, and Y. Xiang, “Quantum image encryption using intra and inter bit permutation based on logistic map,” *IEEE Access*, vol. 7, pp. 6937–6946, 2019, doi: 10.1109/ACCESS.2018.2889896.

[32] E. Winarno, K. Nugroho, P. W. Adi, and D. R. I. M. Setiadi, “Combined interleaved pattern to improve confusion-diffusion image encryption based on hyperchaotic system,” *IEEE Access*, vol. 11, pp. 69005–69021, 2023, doi: 10.1109/ACCESS.2023.3285481.

[33] T. M. Aung, H. H. Naing, and N. N. Hla, “A complex transformation of monoalphabetic cipher to polyalphabetic cipher: (Vigenère-Affine Cipher),” *International Journal of Machine Learning and Computing*, vol. 9, no. 3, pp. 296–303, Jun. 2019, doi: 10.18178/ijmlc.2019.9.3.801.

BIOGRAPHIES OF AUTHORS

Hamid El Bourakkadi received the Master degree in Physics of Materials and Nanostructures from Sidi Mohammed Ben Abdellah University, Morocco, in 2012 and Master degree in Intelligent and Mobile Systems from Sidi Mohammed Ben Abdellah University, Morocco, in 2021, respectively. Currently, Ph.D. degrees in Mathematics and computer science in Mohammed First University, Oujda, Morocco. His research interests include computer science. He can be contacted at email: hamid.elbourakkadi.d23@ump.ac.ma.

Abdelhakim Chemlal received the Master degree in Computer Engineering with a Software Engineering specialization from National School of Applied Science in AL Houceima, Morocco, in Currently, Ph.D. degrees in Matematics and computer science in Mohammed First University, Oujda, Morocco. His research interests include computer science. He can be contacted at email: abdelhakim.chemlal.d23@ump.ac.ma.

Hassan Tabti received the Master degree in Computer science Inforgaphy and Imaging from Sidi Mohammed Ben Abdellah University, Morocco, in 2014. Currently, Ph.D. degrees in Matematics and computer science in Mohammed First University, Fez, Morocco. His research interests include computer science. He can be contacted at email: hassan.tabti1@usmba.ac.ma.

Mourad Kattass received a Master's degree in Robotics and Embedded Systems from the Faculty of Science and Technique, Abdelmalek ESSAADI University, Morocco, in 2020 and a Bachelor's degree in Computer Science, Electronic, Electrotechnical, and Automatic from Sidi Mohammed Ben Abdellah University, Morocco, in 2004, respectively. Currently, Ph.D. degrees in Mathematics and computer science in Mohammed First University, Oujda, Morocco. His research interests include computer science. He can be contacted at email: mourad.kattass@ump.ac.ma.

Abdellatif Jarjar received the Master degree in Fondamental Mathetimatics from Franche Compté Besonçon University, French, in 1987 and Laureate in Mathematics from High Normal School, Morocco, in 1988, respectively. Currently, Searcher in Matematics and computer science in Mohammed First University, Oujda, Morocco. His research interests include computer science. He can be contacted at email: abdoujjar @gmail.com.

Abdelhamid Benazzi Professor and searcher in computer science in Mohammed First University, Oujda, Morocco. His research interests include computer science. He can be contacted at email: a.benazzi @ump.ac.ma.